Demonstration of Two-Atom Entanglement with Ultrafast Optical Pulses

J. D. Wong-Campos,* S. A. Moses, K. G. Johnson, and C. Monroe
Joint Quantum Institute, Joint Center for Quantum Information and Computer Science, and Department of Physics, University of Maryland, College Park, Maryland 20742, USA

(Received 21 September 2017; revised manuscript received 3 November 2017; published 8 December 2017)

We demonstrate quantum entanglement of two trapped atomic ion qubits using a sequence of ultrafast laser pulses. Unlike previous demonstrations of entanglement mediated by the Coulomb interaction, this scheme does not require confinement to the Lamb-Dicke regime and can be less sensitive to ambient noise due to its speed. To elucidate the physics of an ultrafast phase gate, we generate a high entanglement rate using just ten pulses, each of ~20 ps duration, and demonstrate an entangled Bell state with $(76 \pm 1)\%$ fidelity. These results pave the way for entanglement operations within a large collection of qubits by exciting only local modes of motion.

DOI: 10.1103/PhysRevLett.119.230501

Trapped atomic ions are regarded as one of the most mature and promising platforms for quantum information processing [1,2], exhibiting excellent coherence properties [3], near-perfect qubit detection efficiency [4], and high-fidelity entangling gates [5,6]. Entangling operations between multiple ions in a chain typically rely on qubit state-dependent forces that modulate their Coulomb-coupled normal modes of motion [1,7,8]. However, scaling these operations to large qubit numbers in a single chain must account for the increasing complexity of the normal mode spectrum and can result in a gate slowdown [9] or added complexity of the control forces [10].

Here we investigate the fundamental entangling operation of a different scaling approach that uses impulsive optical forces [11–16]. These ultrafast qubit state-dependent kicks occur much faster than the normal mode frequencies of motion and thus can couple through local modes of motion without perturbing spectator trapped ion qubits. This ultrafast approach has the added benefit of being less sensitive to relatively slow noise and is also insensitive to the ions' thermal motion, since it is effectively frozen during the interaction. Unlike other Coulomb-based gates between ions, ultrafast entanglement operations do not require confinement to within the Lamb-Dicke regime, where the motional extent of the ions is smaller than the optical wavelength associated with the force. In this Letter, we show a proof-of-principle demonstration of entanglement between two trapped ion qubits by applying a sequence of ten ultrafast laser pulses and directly show the insensitivity to initial thermal motion outside the Lamb-Dicke regime [17].

In the experiment, we confine two $^{171}Yb^{+}$ atomic ions along the axis of a linear rf (Paul) ion trap [18]. We apply impulsive forces using counterpropagating Raman beams along one of the transverse principal axes of harmonic motion, coupling to both the in-phase center-of-mass (COM) mode at frequency $\omega_C/2\pi = 1.267$ MHz and the out-of-phase relative mode at frequency $\omega_R/2\pi = 1.170$ MHz. To minimize couplings to the other transverse modes, we apply bias voltages to trap electrodes to align one of the principal axes of the trap along the Raman beams. The ion-ion spacing is about 6 μm. The qubit is defined by the ground-state hyperfine levels $|F = 0, m_F = 0\rangle \equiv |\downarrow\rangle$ and $|F = 1, m_F = 0\rangle \equiv |\uparrow\rangle$ of the $^2S_{1/2}$ manifold, separated by $\omega_0/2\pi = 12.64$ GHz. The ions are Doppler cooled on the $^2S_{1/2} \Leftrightarrow {}^2P_{1/2}$ transition at a wavelength of 369.5 nm ($\Gamma/2\pi \sim 20$ MHz), with both COM and relative modes cooled to an average thermal vibrational population of $\bar{n} \sim 10$. Qubit state initialization and detection is performed by optical pumping and state-dependent resonance fluorescence on the same transition with fidelities greater than 99% [19]. Fluorescence is imaged by a 0.6 NA lens with 500× magnification [20], allowing individual qubit state detection with two separated photomultiplier tubes (PMTs).

Impulsive state-dependent forces are provided by $\tau \sim 20$ ps pulses from a mode-locked laser with center wavelength $2\pi/k = 355$ nm and repetition rate $f_{\mathrm{rep}} = 81.42$ MHz that drives stimulated Raman transitions between the qubit levels [21]. As shown in Fig. 1(a), after picking single pulses with an electro-optic Pockels cell, we shape each pulse using a sequence of three delay stages to divide each single pulse into eight subpulses [13]. The pulse train, of total duration ~2.3 ns, is split into two arms with orthogonal linear polarizations and directed onto the ions in a counterpropagating geometry along the transverse direction of motion. Each arm includes an acousto-optic modulator (AOM) that shifts the center frequency of each beam with opposite sign. The net frequency difference between the two arms, which is $\omega_A = \omega_{\mathrm{AOM1}} + \omega_{\mathrm{AOM2}} = 2\pi \times 468.73$ MHz, gives rise to the directionality of the interaction. The delays between the eight subpulses are set in concert with the frequency offset ω_A in order to ensure they coherently add to produce a qubit state-dependent kick (SDK) [14].

For a single trapped ion, the ideal evolution operator from an SDK applied at time t is given by

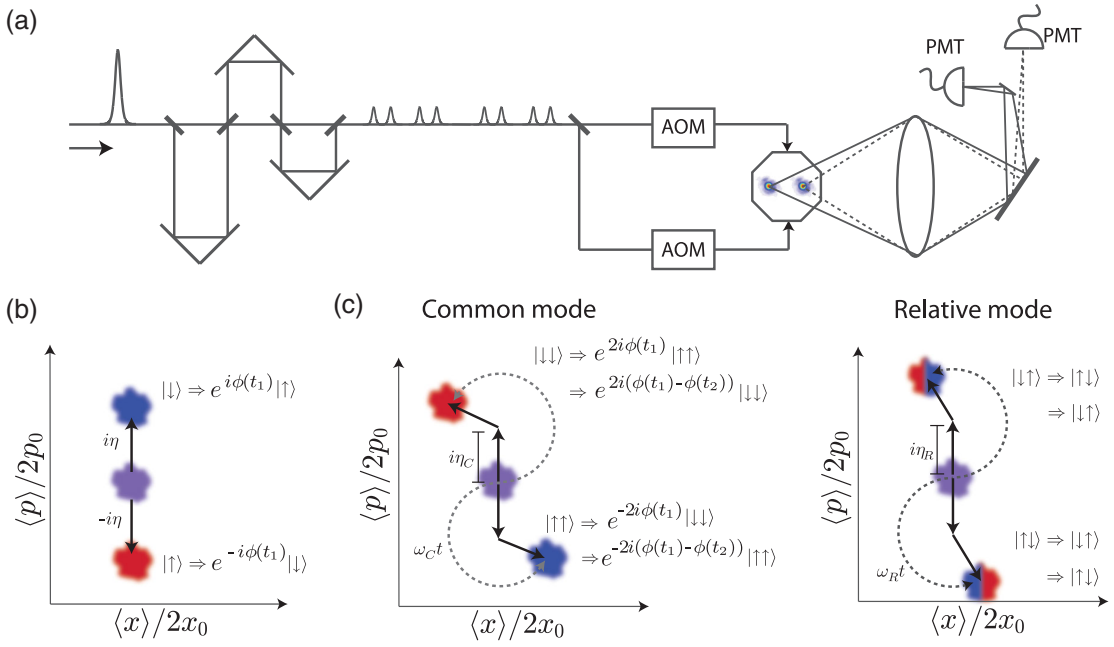

FIG. 1. (a) Experimental schematic. A single pulse from a mode-locked 355 nm laser is divided into eight subpulses by three sequential optical delay stages. The shaped pulse is then split into two paths directed through independent AOMs, used to make the interaction direction dependent. The pulses overlap in space and time at the position of the ions in a counterpropagating lin $\perp$ lin polarization configuration that produces an SDK [21]. Following gate operations, the ion qubits are measured by collecting state-dependent fluorescence from the two ions on respective PMTs when resonant lasers are applied (not shown). (b) Phase space evolution for a single SDK on a single ion. The SDK displaces the momentum of an initial motional state (in purple) by $\pm 2p_0\eta$ in phase space, correlated with the internal spin raising or lowering operator $\sigma_\pm$ in the ion. (c) Phase space evolution for two collective modes of motion under a sequence comprised of an SDK at time t_1, free evolution, and a second SDK at time t_2, in frames rotating at the respective mode frequencies. Each SDK imparts a phase depending on the magnitude of the momentum kick and the coherent state before the kick [see Eq. (3)], as well as a laser phase $2\phi(t)[-2\phi(t)]$ on the $|\downarrow\downarrow\rangle$ ($|\uparrow\uparrow\rangle$) states [see Eq. (4)]. In addition, the motional states acquire a phase from the free evolution [see Eq. (2)]. Because the evolution is depicted in the rotating frame, the direction of an SDK depends on the time elapsed since the previous SDK.

$e^{i\phi(t)}\hat{\mathcal{D}}(i\eta)\hat{\sigma}_+ + e^{-i\phi(t)}\hat{\mathcal{D}}(-i\eta)\hat{\sigma}_-$. The phase $\phi(t) = \omega_A t + \Delta\phi_L$ is related to the AOM frequency and the difference in optical phase $\Delta\phi_L$ between the two arms, assumed to be constant during the interaction. The raising and lowering operators $\hat{\sigma}_\pm$ act on the qubit, and the displacement operator $\hat{\mathcal{D}}(\pm i\eta)$ acts on the motional state of the ion along the axis of transverse motion, translating the momentum in phase space by $\Delta p = \pm\hbar(\Delta k) = \pm 2p_0\eta$. Here $\Delta k = 2k$ is the wave vector difference between the counterpropagating beams, and $p_0 = \sqrt{m\hbar\omega/2}$ is the zero-point momentum spread of harmonic motion at frequency ω for an ion of mass m ($x_0 = \hbar/2p_0$ is the zero-point position spread). The Lamb-Dicke parameter $\eta = \hbar\Delta k/(2p_0) \approx 0.17$ thus parametrizes the momentum kick in natural units. In contrast to conventional forces applied in the resolved sideband regime [22], the impulsive SDK is about 300 times faster than the oscillation period and does not rely on confinement to the Lamb-Dicke regime.

The action of an SDK on two ions is given by

$$\hat{U}_{\mathrm{SDK}}(t) = e^{2i\phi(t)}\hat{\sigma}_{1+}\hat{\sigma}_{2+}\hat{\mathcal{D}}_C(i\eta_C) + e^{-2i\phi(t)}\hat{\sigma}_{1-}\hat{\sigma}_{2-}\hat{\mathcal{D}}_C(-i\eta_C) + \hat{\sigma}_{1+}\hat{\sigma}_{2-}\hat{\mathcal{D}}_R(i\eta_R) + \hat{\sigma}_{1-}\hat{\sigma}_{2+}\hat{\mathcal{D}}_R(-i\eta_R), \quad (1)$$

with spin operators for each ion and displacement operators for each mode. The Lamb-Dicke parameters for the COM and relative modes are $\eta_C = \sqrt{2}\eta = 0.24$ and $\eta_R = \sqrt{2\omega_C/\omega_R}\eta = 0.25$, respectively. Because of their distinct displacement amplitudes and frequencies, the COM and relative modes trace distinct paths in phase space when subjected to a sequence of SDKs interspersed with free evolution. Figure 1(c) shows the trajectories of the two modes in frames rotating at the respective mode frequencies, where the SDK displacement for each mode m has magnitude η_m along an axis rotated by angle $\omega_m t$ with respect to the previous kick after elapsed time t.

A sequence of SDK pulses indexed to uniform time steps of duration $T = 1/f_{\mathrm{rep}}$ can be expressed by N displacement indices $\{b_1, b_2, \ldots, b_N\}$ with $b_n = \pm 1$ for a kick and $b_n = 0$ corresponding to a wait (no pulse). Since two successive SDKs undo each other, whether b is $+1$ or -1 for a particular kick depends on the sign associated with the previous kick and whether the beam direction, defined by which beam is shifted up in frequency, is the same or reversed $[\Delta k \to -\Delta k, \phi(t) \to -\phi(t)]$. Since the frequency of the two beams is correlated with the polarization, we can reverse the beam direction with a second Pockels cell [23].

If the beam direction stays the same, then b switches signs; if the direction is reversed, then b stays the same sign. So for a sequence where all of the pulses have the same orientation, the b's will alternate between $+1$ and -1. This sequence leads to displacements of initial coherent states for each mode m from $|\alpha_0\rangle_m$ to $e^{i\phi_m}|\alpha\rangle_m$, with [11]

$$\alpha = e^{-iN\omega_m T}\left(\alpha_0 + i\sum_{n=1}^{N}\eta_m b_n e^{in\omega_m T}\right),$$
$$\phi_m = \mathrm{Re}\left(\alpha_0\sum_{n=1}^{N}\eta_m b_n e^{-in\omega_m T}\right) + \sum_{n=2}^{N}\sum_{j=1}^{n-1}\eta_m^2 b_n b_j \sin[\omega_m T(n-j)]. \quad (2)$$

We design pulse sequences $\{b_n\}$ so that the sum in Eq. (2) vanishes and both motional phase spaces close. Given an even number of pulses, this produces a phase gate described with truth table

$$|\downarrow\downarrow\rangle \Rightarrow |\downarrow\downarrow\rangle e^{i(\Phi_g+\gamma)}, \quad |\downarrow\uparrow\rangle \Rightarrow |\downarrow\uparrow\rangle,$$
$$|\uparrow\downarrow\rangle \Rightarrow |\uparrow\downarrow\rangle, \quad |\uparrow\uparrow\rangle \Rightarrow |\uparrow\uparrow\rangle e^{i(\Phi_g-\gamma)}. \quad (3)$$

The nonlinear geometric phase $\Phi_g = \phi_C - \phi_R$ is set to $\pi/2$ for maximum entanglement. The residual linear phase from the series of optical kicks is

$$\gamma = 2\omega_A T\sum_{n=1}^{N} n b_n + 2\Delta\phi_L\sum_{n=1}^{N} b_n, \quad (4)$$

assumed to be constant throughout the gate sequence but varying from one experiment to the next. In order to eliminate the dependence on $\Delta\phi_L$, we must utilize sequences with an even number of pulses where the sum of the b's is 0.

Here, we implement a quantum gate with fast pulses by finding gate sequences with the least number of SDKs, without reversing the beam directions (so the nonzero b's alternate between $+1$ and -1). For N_p individual pulses separated in time by an integer multiple M of the laser pulse period T, the condition for closing phase spaces is similar to the tracing of a regular polygon in the complex plane. We achieve the largest nonlinear gate phase for a given number of pulses by driving the COM and relative modes in opposite directions in phase space so that $\phi_R \approx -\phi_C$.

Using the above trap parameters with $N_p = 10$, we find that the phase space trajectories of COM and relative modes trace out regular decagons of opposite circulation for

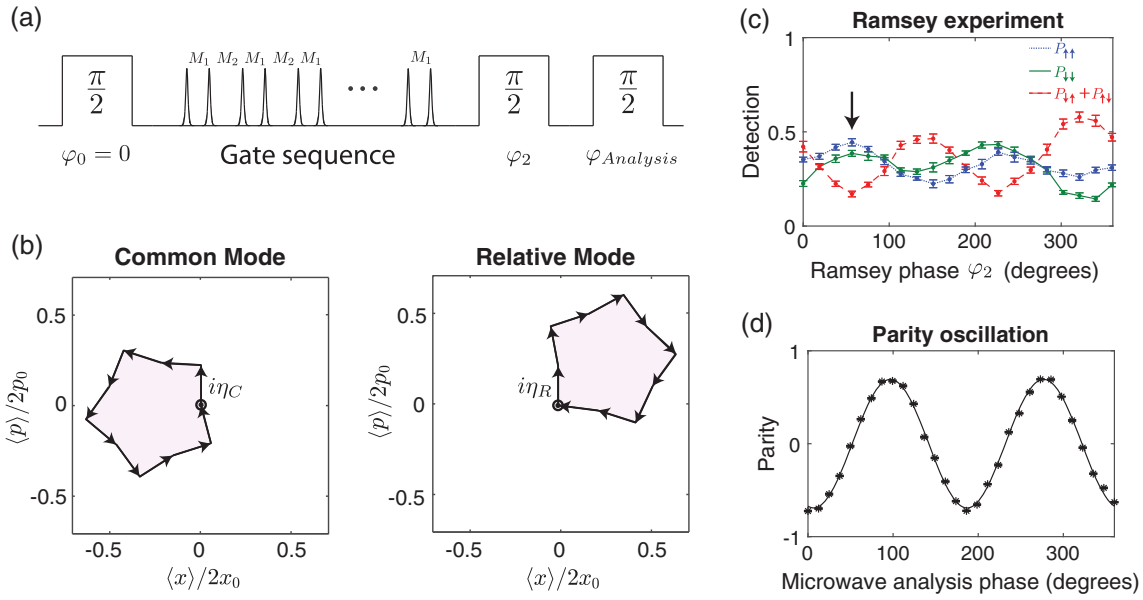

FIG. 2. (a) The gate sequence is applied within a Ramsey experiment. The entangling gate contains five repetitions of a sequence consisting of a single SDK ($b_n = 1$), followed by a wait of M_1 time steps ($b_n = 0$), another SDK ($b_n = -1$), and a final wait of M_2 time steps. (b) Depiction of the trajectories followed by the COM and relative modes for a fully entangling sequence. They follow opposite circulations and enclose similar areas, and the sum leads to the gate phase. (c) We choose ϕ_2 such that we maximize $P_{\uparrow\uparrow}$, $P_{\downarrow\downarrow}$ and minimize $P_{\downarrow\uparrow}$, $P_{\uparrow\downarrow}$ (black arrow). The population in $|\uparrow\downarrow\rangle$ and $|\downarrow\uparrow\rangle$ is due mostly to SDK infidelity causing single-particle coherences. Amplitude differences of the peaks in the $P_{\downarrow\uparrow} + P_{\uparrow\downarrow}$ signal are likely caused by microwave power calibration errors. (d) The parity oscillation amplitude after choosing the value of ϕ_2 corresponding to the black arrow in (c) is proportional to $2\rho_{\uparrow\uparrow,\downarrow\downarrow}$, which allows us to compute the fidelity. The best parity oscillation amplitude achieved is 0.69(1), leading to a final gate fidelity of 76(1)%. The error bars reflect the statistical uncertainty and for (d) are typically smaller than the points.

$M = 166$, with corresponding gate phase $\Phi_g = \pi/1.67$. Other values of Φ_g can be realized by alternating between two different integer multiples of the pulse periods, M_1 and M_2, such that $M_1 + M_2 = 2M$. This deforms the trajectories to decagons with two distinct vertex angles [see Figs. 2(b) and 3(a)], allowing the fine-tuning of Φ_g. For $M_1 = 175$ and $M_2 = 157$, we find $\Phi_g = \pi/2.06$, nearly a fully entangling gate in a total duration of $(N_p M - M_2)T = 18.5$ μs. There are many more types of pulse solutions with even more complex polygonal trajectories given the delay times between pulses.

We characterize the phase gate by applying the gate operation within a three-pulse Ramsey interferometer on the qubits. We start the sequence by optically pumping the ions to the state $|\downarrow\downarrow\rangle$. A first microwave $\pi/2$ pulse rotates both spins to populate an equal superposition of all four basis states. The entangling laser pulse sequence is then applied, which according to the truth table [Eq. (4)] should ideally produce the state

$$\Psi_e = \frac{e^{i\Phi_g}}{2}(e^{i\gamma}|\downarrow\downarrow\rangle + e^{-i\gamma}|\uparrow\uparrow\rangle) - \frac{1}{2}(|\uparrow\downarrow\rangle + |\downarrow\uparrow\rangle), \quad (5)$$

where in the above expression we have suppressed the motional state, since both phase spaces should be closed at this point.

A second $\pi/2$ microwave Ramsey pulse (with phase ϕ_2 with respect to the first pulse) is then applied. We choose its phase to ideally create the state

$$\Psi_f = \frac{e^{-i\gamma}}{2}(e^{i\Phi_g} - 1)|\downarrow\downarrow\rangle + \frac{e^{i\gamma}}{2}(e^{i\Phi_g} + 1)|\uparrow\uparrow\rangle. \quad (6)$$

We experimentally determine the appropriate phase of the second Ramsey $\pi/2$ pulse by maximizing the populations $P_{\uparrow\uparrow}$ and $P_{\downarrow\downarrow}$ of the even parity states, as shown in the Ramsey fringes of Fig. 2(c).

In order to verify the coherence of the above entangled state, we apply a third $\pi/2$ "analysis pulse" and measure the parity of the two qubits as a function of the phase of this last pulse, as shown in Fig. 2(d). The parity oscillates with twice the period of a single spin, and the contrast C of the oscillation reveals the coherence between the entangled superposition in Eq. (6). The state fidelity with respect to the ideal Bell state is then $F = (P_{\uparrow\uparrow} + P_{\downarrow\downarrow} + C)/2$ [25]. We measure a Bell state fidelity of $F = 76(1)\%$.

As a further validation of our control over various gate sequences, we vary the gate phase Φ_g by changing the number of pulses M_1 and M_2 over a wider range. In Fig. 3(a), we show a measurement of the parity oscillation contrast C for different values of Φ_g. The measured parity oscillation amplitude for each gate sequence agrees well with the expected $\sin\Phi_g$ dependence. Finally, we note that the linear phase γ can be regarded as a constant offset phase in the above data and does not affect the amount of entanglement or its diagnosis.

The entangling gate presented here is fundamentally different than the Mølmer-Sørensen [8] and Cirac-Zoller [7] gates for trapped ions, since individual motional modes are not resolved. Moreover, the (thermal) motion of the ions occupies a spatial extent of $x_0\sqrt{2\bar{n}+1} \approx 0.8/\Delta k$, outside the Lamb-Dicke regime.

We implemented a faster gate by dynamically switching the laser beam wave vector difference Δk by inserting a second electro-optic Pockels cell after the two AOMs. The

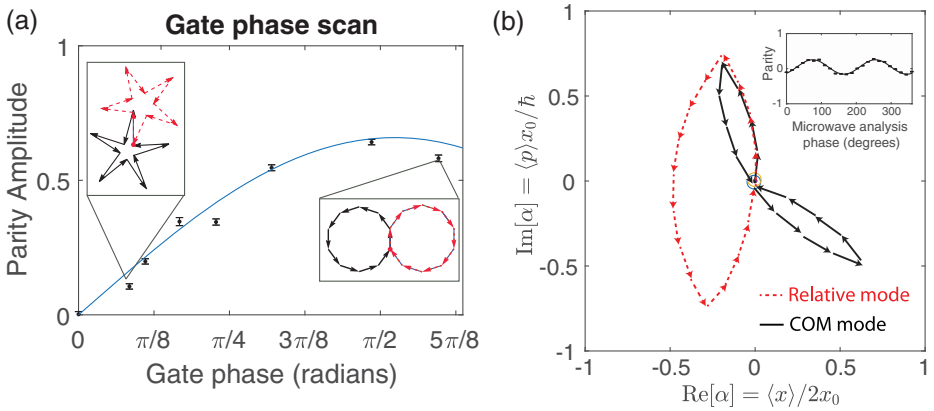

FIG. 3. (a) Measured parity oscillation amplitude for various values of the gate phase Φ_g, which should be proportional to $\sin\Phi_g$ (solid blue line). The gate phase is modified by changing the pulse schedule given by the integers M_1 and M_2 (see the main text). The insets show phase space trajectories for the COM (black solid curves) and relative (red dashed curves) modes for $\Phi_g = \pi/1.67$ (right) and $\Phi_g = \pi/11.9$ (left). The fidelity of the entangled state produced in each case, referenced to the ideal state $\Psi_f(\Phi_g)$ in Eq. (6), is roughly 0.7 for all the measurements. (b) Pulse sequence for a faster sequence, where the kicks along the arms of the trajectory are switched each time, and there is trap evolution to round the corners. See Supplemental Material [24] for experimental details, including the pulse schedule. The inset shows the parity oscillation. Because there are more pulses, the gate phase is less than $\pi/2$, and there are additional infidelities introduced by the switching, the amplitude of the parity oscillation is significantly smaller than that in Fig. 2. The total gate time is about 1.95 μs.

sequence is shown in Fig. 3(b), consists of 16 SDKs, and has a total duration of 1.95 μs for $\Phi_g \approx \pi/2.4$. The trap frequencies were slightly lower than those used for the previous experiment ($\omega_C = 2\pi \times 1.13$ MHz and $\omega_R = 2\pi \times 1.02$ MHz) to better close both phase spaces. As expected, the larger number of pulses and additional infidelities introduced by the switching operation [23] make the amplitude of the parity oscillation significantly less than for the sequence described earlier. We note that faster gate sequence solutions that are fully entangling would require more SDKs or lower trap frequencies.

The gate infidelities in the demonstration presented here are due to infidelities in the SDK, which can possibly arise from a variety of sources, including coupling to unwanted modes or the $|1, \pm 1\rangle$ states, or issues related to the pulse picking with a Pockels cell in the ultraviolet. In the future, it may be possible to achieve the same ultrafast control with infrared optical sources instead of ultraviolet lasers by frequency-up-converting to the UV after pulse shaping, pulse switching, or exploiting a longer-wavelength atomic transition for the SDK.

Acknowledgments

This work is supported by the U.S. Army Research Office and the National Science Foundation Physics Frontier Center at the Joint Quantum Institute.

*jwongcam@umd.edu

[1] R. Blatt and D. Wineland, Nature (London) **453**, 1008 (2008).
[2] C. Monroe and J. Kim, Science **339**, 1164 (2013).
[3] P. T. Fisk, M. J. Sellars, M. A. Lawn, and G. Coles, IEEE Trans. Ultrason. Ferroelectr. Freq. Control **44**, 344 (1997).
[4] A. Myerson, D. Szwer, S. Webster, D. Allcock, M. Curtis, G. Imreh, J. Sherman, D. Stacey, A. Steane, and D. Lucas, Phys. Rev. Lett. **100**, 200502 (2008).
[5] C. J. Ballance, T. P. Harty, N. M. Linke, M. A. Sepiol, and D. M. Lucas, Phys. Rev. Lett. **117**, 060504 (2016).
[6] J. P. Gaebler *et al.*, Phys. Rev. Lett. **117**, 060505 (2016).
[7] J. I. Cirac and P. Zoller, Phys. Rev. Lett. **74**, 4091 (1995).
[8] K. Mølmer and A. Sørensen, Phys. Rev. Lett. **82**, 1835 (1999).
[9] T. Monz, D. Nigg, E. A. Martinez, M. F. Brandl, P. Schindler, R. Rines, S. X. Wang, I. L. Chuang, and R. Blatt, Science **351**, 1068 (2016).
[10] S. Debnath, N. M. Linke, C. Figgatt, K. A. Landsman, K. Wright, and C. Monroe, Nature (London) **536**, 63 (2016).
[11] J. J. García-Ripoll, P. Zoller, and J. I. Cirac, Phys. Rev. Lett. **91**, 157901 (2003).
[12] L.-M. Duan, Phys. Rev. Lett. **93**, 100502 (2004).
[13] J. Mizrahi, C. Senko, B. Neyenhuis, K. G. Johnson, W. C. Campbell, C. W. S. Conover, and C. Monroe, Phys. Rev. Lett. **110**, 203001 (2013).
[14] J. Mizrahi, B. Neyenhuis, K. G. Johnson, W. C. Campbell, C. Senko, D. Hayes, and C. Monroe, Appl. Phys. B **114**, 45 (2014).
[15] C. D. B. Bentley, A. R. R. Carvalho, D. Kielpinski, and J. J. Hope, New J. Phys. **15**, 043006 (2013).
[16] M. Palmero, S. Martínez-Garaot, D. Leibfried, D. J. Wineland, and J. G. Muga, Phys. Rev. A **95**, 022328 (2017).
[17] K. G. Johnson, B. Neyenhuis, J. Mizrahi, J. D. Wong-Campos, and C. Monroe, Phys. Rev. Lett. **115**, 213001 (2015).
[18] K. G. Johnson, J. D. Wong-Campos, A. Restelli, K. A. Landsman, B. Neyenhuis, J. Mizrahi, and C. Monroe, Rev. Sci. Instrum. **87**, 053110 (2016).
[19] S. Olmschenk, K. C. Younge, D. L. Moehring, D. Matsukevich, P. Maunz, and C. Monroe, Phys. Rev. A **76**, 052314 (2007).
[20] J. D. Wong-Campos, K. G. Johnson, B. Neyenhuis, J. Mizrahi, and C. Monroe, Nat. Photonics **10**, 606 (2016).
[21] W. C. Campbell, J. Mizrahi, Q. Quraishi, C. Senko, D. Hayes, D. Hucul, D. N. Matsukevich, P. Maunz, and C. Monroe, Phys. Rev. Lett. **105**, 090502 (2010).
[22] D. Leibfried, R. Blatt, C. Monroe, and D. Wineland, Rev. Mod. Phys. **75**, 281 (2003).
[23] K. G. Johnson, J. D. Wong-Campos, B. Neyenhuis, J. Mizrahi, and C. Monroe, Nat. Commun. **8**, 697 (2017).
[24] See Supplemental Material at http://link.aps.org/supplemental/10.1103/PhysRevLett.119.230501 for a more detailed description of the rotating phase space picture, the phase space trajectories for the gate sequences, and the limitations of the SDK fidelity.
[25] C. A. Sackett *et al.*, Nature (London) **404**, 256 (2000).